Application-Oriented System-Level Optimization Method for Switched Reluctance Motor Drive Systems

Kaikai Diao
Automotive Engineering Research Institute
Jiangsu University
Zhenjiang, China
diaokaikai@163.com

Xiaodong Sun
Automotive Engineering Research Institute
Jiangsu University
Zhenjiang, China
xdsun@ujs.edu.cn

Gang Lei
School of Electrical and Data Engineering
University of Technology Sydney
Sydney, Austria
Gang.Lei@uts.edu.au

Youguang Guo
School of Electrical and Data Engineering
University of Technology Sydney
Sydney, Austria
Youguang.Guo-1@uts.edu.au

Jianguo Zhu
School of Electrical and Information Engineering
University of Sydney
Sydney, Austria
jianguo.zhu@sydney.edu.au

***Abstract*—In this paper, a novel application-oriented system-level optimization method is proposed for switched reluctance motor (SRM) drive systems. First, the multiobjective optimization model is defined according to the design requirements. Then, all the parameters of the motor and controller are divided into three subspaces according to the sensitivity results on the defined objectives. Finally, the optimization of each subspace is performed sequentially by using the approximate models and advanced genetic algorithm, and the best solution can be selected from the Pareto optimal solutions. To verify the effectiveness of the proposed method, an SRM drive system with a segmented-rotor SRM and the angle position control method is investigated. This is a high-dimensional system-level optimization problem with ten parameters. The computational cost can be greatly reduced without the sacrifice of accuracy. From the discussion, it can be found that the proposed multiobjective system-level optimization method can achieve high efficiency and low torque ripple. Besides, it provides alternative solutions for applications with different output power demands.**

***Keywords*—Optimization method, switched reluctance motor, system-level design optimization.**

I. INTRODUCTION

Switching reluctance motors (SRMs) are witnessing increasing attention due to the advantages of high reliability and robustness, low manufacturing cost, and the absence of permanent magnet [1-3]. Compared with the other types of motors, SRMs suffer from higher torque ripple contributed to the nonlinear coupling between inductance, phase current, and rotor position [4-6]. The design optimization process is a common approach to reduce torque ripple and improve comprehensive performances. The problem of single-objective optimization is the potential downgrading of other significant performance indices. However, in the actual application, there always exist multiple design requirements, such as maximizing output torque and efficiency, and minimizing the torque ripple. Therefore, the implementation of multiobjective optimization on SRMs is more suitable to accommodate the requirements for different applications [7], [8].

Previous works on the multiobjective optimization of SRMs mainly focus on geometric parameters by selecting approximate stator and rotor sizes, which are mostly on the component level rather than the system level [9-12]. For example, in [13], a sample SRM with multiple optimizations was carried out, and the optimization variables from all the geometric parameters were selected according to their influence on objectives. However, this method only achieves the best structure of the motor. Since it did not consider the control parameters, it cannot guarantee the best solution for the drive system. Aside from the motor aspect, a multiobjective optimization method has also been conducted on the control aspect of SRMs [14]. Several kinds of research have been performed on both motor and control aspects simultaneously. As reported in [15], to obtain the best performance of electric drive systems, the optimization should contain both the motor level and control level. Thus, it is meaningful to conduct the optimization for the whole drive system. Recently, a system-level design optimization method for SRM drive system was proposed in [16], the optimal solution was selected by a selection criterion which incorporating the optimization objectives by weighting factors. The demands of meeting the design requirements were realized by choosing different values of weighting factors, which is not convenient and intuitive in the application-oriented optimization problem.

This paper presents a novel application-oriented system-level optimization method for SRM drive systems considering

This work was supported by the National Natural Science Foundation of China under Project 51875261, the Natural Science Foundation of Jiangsu Province of China under Projects BK20180046 and BK20170071, and the Postgraduate Research & Practice Innovation Program of Jiangsu Province under Project KYCX20_2844.

multiple optimization objectives. Both the motor and control aspects are optimized by the multiobjective optimization method. Besides, the multilevel method is performed to reduce the computation cost and improve optimization efficiency. A suitable solution can be selected from the Pareto optimal solutions with different application demands. The remainder of this paper is organized as follows. Section II presents the proposed method. Section III investigates an example study for the design optimization of a segmented-rotor switched reluctance motor (SSRM) and its control approach. Specific implementation and results are provided in Section IV, followed by the conclusion in Section V.

II. Application-oriented System-Level Optimization Method

Fig. 1 shows the flowchart of the proposed application-oriented system-level optimization method for SRM drive systems. This method includes multiobjective, multilevel, and system-level optimization methodologies, and it can be divided into six steps as follows.

Step 1: Build the multiobjective optimization model considering the system parameters for the SRM drive systems.

The multiobjective model can be defined as

$$\begin{aligned} \min: \quad & \begin{cases} f_1(\mathbf{x}_s) \\ f_2(\mathbf{x}_s) \\ \quad \vdots \\ f_m(\mathbf{x}_s) \end{cases} \\ s.t. \quad & g_i(\mathbf{x}_s) \le 0, i = 1,2,\ldots n \\ & \mathbf{x}_{sl} \le \mathbf{x}_s \le \mathbf{x}_{su} \end{aligned} \tag{1}$$

where $\mathbf{x}_s$, f, g_i are the design parameter vector, objective, and constraints of the motor, respectively, $\mathbf{x}_s$ consists of motor parameter vector and control parameter vector, $\mathbf{x}_{sl}$ and $\mathbf{x}_{su}$ are the lower boundary and upper boundary, respectively.

Step 2: Carry out sensitivity analysis for all parameters of the SRM drive system, including motor level and control level.

In a high dimensional design optimization problem, some design parameters related to the objectives are more significant than others. The sensitivity analysis process is utilized to achieve the potential influences of each design variable on the optimization objectives. Therefore, the high dimensional design space can be divided into several low dimensional design spaces in terms of their sensitivity results.

Step 3: Divide the system parameters into three subspaces X_1, X_2, and X_3, where X_1, X_2, and X_3 represent the highly significant, significant, and non-significant subspaces of system design parameters, respectively.

The principle of the division is decided by the results of influences on the defined optimization objectives in (1). The results can be achieved from the sensitivity analysis proposed in the last step.

Step 4: Optimize X_1. In the implementation, parameters in X_2 and X_3 are fixed as the initial values. The Pareto optimal solution set of X_1 is obtained in this step, and then several points are selected to the next step to achieve the Pareto optimal solution set of X_2.

Step 5: Optimize X_2. Similar to the last step, the Pareto optimal solution set of X_2 is obtained in this step based on the selected values of parameters in X_1, then, several points with definite values of X_1 and X_2 are sent to the next step.

Step 6: Optimize X_3. The values of parameters in X_1 and X_2 are fixed as selected. The final optimal points can be chosen from Pareto solutions to this subspace.

Furthermore, it should be noted that in steps 5 and 6, as more than one optimal solution are selected, several Pareto optimal solutions will be obtained corresponding to each selected point in the previous step. The best way to solve this problem is to merge all the Pareto optimal solutions into one picture, which will be more intuitive.

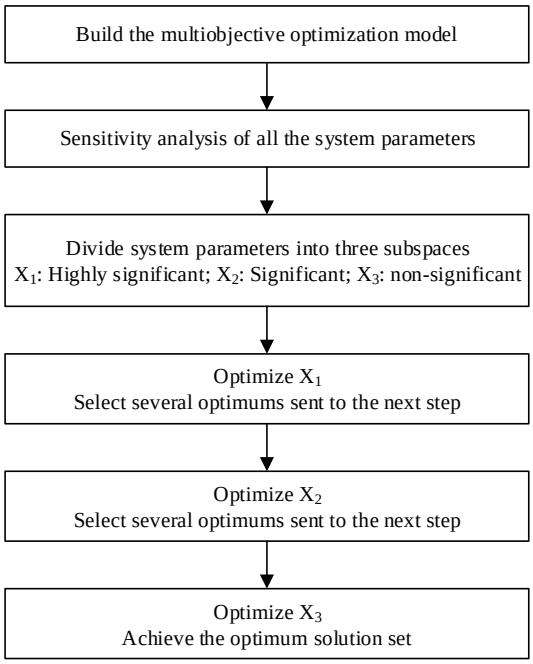

Fig. 1. Flowchart of application-oriented system-level optimization method for SRM drive systems.

III. Example of an SRM Drive System

In this example, an SRM drive system consisting of an SSRM and the APC control is set as an example to investigate the proposed optimization method. The specifications of the SSRM are presented in Table I.

TABLE I
Specifications of the SSRM

Parameters	Unit	value
Rated power	kW	1.8
Rated speed	r/min	6000
Rated voltage	V	60
Efficiency	%	0.85
Outer diameter	mm	128
Axial length	mm	80

Fig. 2 shows the topology of the SSRM. The stator poles are divided into excited poles and auxiliary poles. The excited poles wrapped by the coils provide the flux linkage while the auxiliary poles play the role of the flux return path without any windings. The benefit of this structure is that it can provide a short flux path, and thus exhibits higher efficiency and lower core loss compared with the common double-salient structure. The descriptions of each parameter and their values are presented in Table II. In this application, the optimization model can be defined as follows.

$$\begin{aligned} \min: \quad & \begin{cases} f_1(\mathbf{x}_s) = -T_{avg} \\ f_2(\mathbf{x}_s) = P_{loss} \\ f_3(\mathbf{x}_s) = T_{ripple} \end{cases} \\ s.t. \quad & g_1(\mathbf{x}_s) = 0.85 - \eta \le 0 \\ & g_2(\mathbf{x}_s) = sf - 0.6 \le 0 \\ & g_3(\mathbf{x}_s) = J_c - 6 \le 0 \\ & \mathbf{x}_{sl} \le \mathbf{x}_s \le \mathbf{x}_{su} \end{aligned} \tag{2}$$

where T_{avg}, $P_{loss,}$ and T_{ripple} are the three optimization objectives, which represent the average output torque, average loss and torque ripple, respectively. η, P_{out}, sf and J_c represent the efficiency, output power, slot fill factor and current density, respectively.

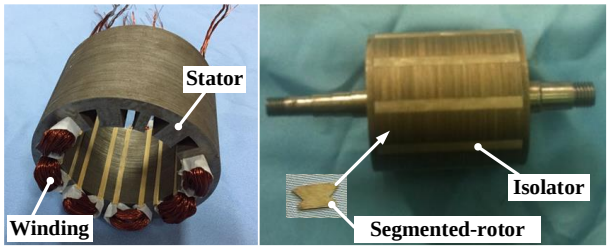

Fig. 2. The topology of the SSRM.

TABLE II
INITIAL DESIGN DIMENSIONS OF THE SSRM

Par.	Description	Unit	Value
N_{ph}	Number of phases	-	4
N_s	Number of stator poles	-	16
N_r	Number of rotor poles	-	10
D_{so}	Stator outer diameter	mm	128
l	Axial length	mm	80
D_{ro}	Rotor outer diameter	mm	82
β_{s1}	Excited stator pole arc	deg.	21.375
β_{s2}	Auxiliary stator pole arc	deg.	10.688
β_r	Rotor pole arc	deg.	26.64
L_{sy}	Stator yoke	mm	7
h_{cr}	Height of segmented rotor	mm	5.5
g	Air gap	mm	0.25
N	Number of turns	-	24
θ_{on}	Turn-on angle	deg.	-3
θ_{off}	Turn-off angle	deg	12

IV. IMPLEMENTATION AND RESULTS

In the implementation process, a large number of finite element modes (FEMs) will be established. And the whole discussion is based on the data from FEMs. Thus, it is necessary to verify the reliability of FEM at first. Second, local sensitivity analysis is performed to divide all the parameters into three subspaces, which is beneficial to release the computational cost. Then, the approximate model of each subspace is built by using the Kriging model, and Pareto optimal solutions are achieved by the advanced algorithm NSGA-II. The accuracy of the Kriging model will be verified by several randomly selected points. Finally, a comparison between the optimal sets and the initial design is investigated, and the results are further presented and discussed.

A. Verification of FEM

The platform of the investigated SSRM drive system is presented in Fig. 3. The comparison between simulation and measured results of flux linkage and torque are shown in Figs. 4 and 5, respectively. All the measured results can verify the reliability of the simulation, which built the foundation of the FEM-based optimization process.

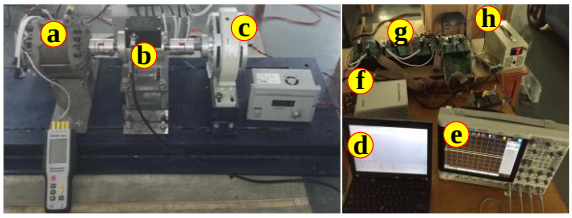

Fig. 3. The platform of the investigated SSRM drive system. (a) The 16/10 SSRM. (b) Torque and speed sensor. (c) Magnetic power brake. (d) PC. (e) Oscilloscope. (f) dSPACE. (g) Powder converter and driving circuit. (h) Power supply.

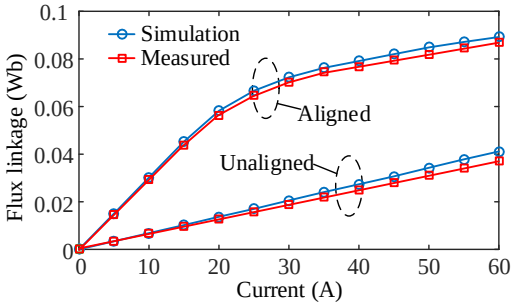

Fig. 4. Simulation and measured results of flux linkage.

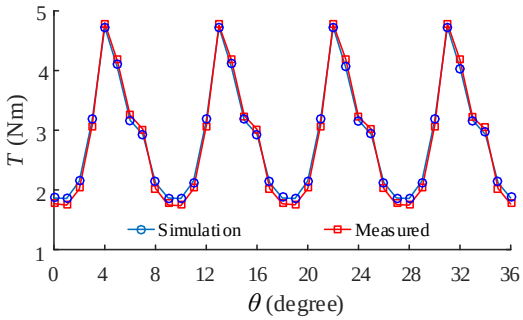

Fig. 5. Output torque comparison of the experimental and simulation results under APC at speed 6000 r/min.

B. *Sensitivity analysis*

Fig. 6 shows the local sensitivity analysis results of the ten parameters. Three subspaces are determined according to the sensitivity influence on torque, loss and torque ripple. Subspace X_1 includes parameters D_{ro}, β_r and N, subspace X_2 includes parameters β_{s1}, β_{s2} and θ_{off}, and subspace X_3 includes parameters θ_{on}, L_{sy}, h_{cr}, and g.

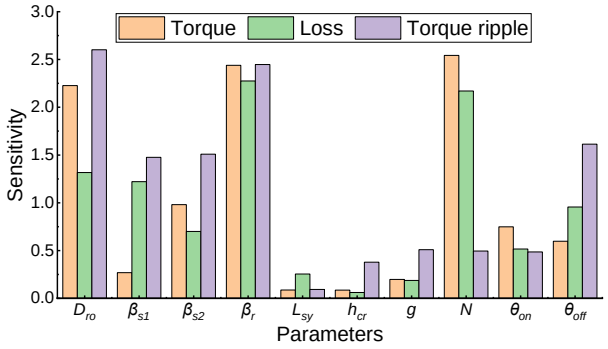

Fig. 6. Local sensitivity indices of torque, loss, and torque ripple.

C. *Multilevel optimization*

The parameters in the subspace X_1 are highly significant to the overall performances of the drive system, and they are optimized at the first level. In this level, 1001 (11x13x7, where 11, 13 and 7 are the sampling numbers of parameters D_{ro}, β_r, and N, respectively) FEM samples in total are established for the optimization. The Pareto optimal solutions of this level are shown in Fig. 7(a). Three regions have been divided according to the torque values. Regions 1, 2 and 3 represent the optimal solutions in the torque ranges 5~7 Nm, 3~5 Nm, and 1~3 Nm, respectively. Then, three optimal points from each region, i.e., Point 1", Point 2" and Point 3", have been selected for the implementation of level 2 optimization.

After the optimization of level 1, significant parameters in the subspace X_2 will be optimized under the fixed values of parameters in X_1. For each selected point in X_1, 150 (6x5x5, where 6, 5, and 5 mean the sampling numbers of parameters β_{s1}, β_{s2} and θ_{off}, respectively) FEM samples in total are established, and the corresponding Pareto solutions can be achieved during the optimization of level 2. Three sets of Pareto optimal solutions corresponding to Point 1", Point 2" and Point 3" can be obtained. In this paper, the three sets are merged into one set, and the Pareto optimal solutions at this level are shown in Fig. 7(b). Besides, three optimal points, namely Point 1', Point 2' and Point 3' are sent to the next optimization step. Compared to Fig.7(a), it can be found that torque ripple has been greatly reduced after the optimization of level 2.

Similarly, for each selected point in X_2, 180 (3x3x5x4, where 3, 3, 5 and 4 mean the numbers of values of θ_{on}, L_{sy}, h_{cr}, and g, respectively) FEM samples are required. The three sets of Pareto optimal solutions in the optimization of level 3 are merged into one figure, as shown in Fig. 7(c). The final three optimal points in Fig. 7(c), i.e., Point 1, Point 2 and Point 3, are selected after the optimization of parameters in X_3. Point k (k=1,2,3) has the same values of parameters in X_1 with Point k" and the same values of parameters in X_2 with Point k'. Specific values of the parameters of the three points are presented in Table III.

TABLE III
Optimization Results

Par.	Unit	Point 1	Point 2	Point 3
D_{ro}	mm	84.86	84.79	85.00
β_{s1}	deg.	21.47	21.50	21.50
β_{s2}	deg.	9.92	9.27	10.23
β_r	deg.	24.26	26.62	30.00
L_{sy}	mm	7.71	5.00	8.86
h_{cr}	mm	6.04	4.00	6.84
g	mm	0.26	0.35	0.28
N	-	21	22	26
θ_{on}	deg.	-3.10	-3.50	-2.90
θ_{off}	deg	11.00	11.14	11.11
T_{avg}	Nm	6.03	4.36	2.08
P_{out}	kW	3.79	2.74	1.31
P_{loss}	W	328.44	283.72	110.50
η	%	92.03	90.62	92.22
T_{ripple}	%	83.34	51.75	114.90

On the other hand, multilevel optimization can greatly improve the computation efficiency for the whole system optimization. The single-level optimization, for example, if the Kriging model is employed, the required FEM samples (1001*150*180) will be much larger. Regarding the multilevel optimization, if one optimal point is selected, only 1331 (1001+150+180) FEM samples are required for the multiobjective optimization of this drive system. Therefore, the proposed multilevel optimization method can greatly reduce the burden and cost of computation, especially for the optimization of the high-dimensional structure.

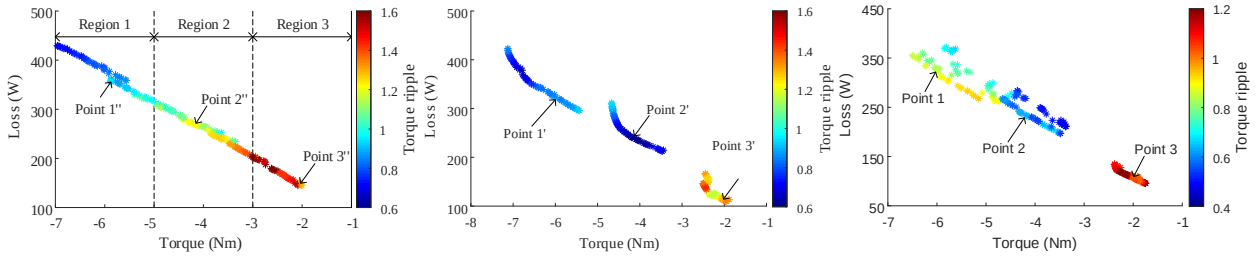

(a) (b) (c)

Fig. 7. Pareto optimal solutions of (a) level 1, (b) level 2, and (c) level 3.

D. *Verification of Kriging model*

After the optimization process, three points have been selected, thus, the results between the Kriging model and FEM of these points are compared to verify the effectiveness of the approximate model. The FEM results have been verified by the comparison with the experiment results, as mentioned above. Thus, the accuracy of the Kriging model can be verified by the FEM results.

TABLE IV
COMPARISON BETWEEN KRIGING MODEL AND FEM

Par.	Point 1		Point 2		Point 3	
	Krig.	FEM	Krig.	FEM	Krig.	FEM
T_{avg} (Nm)	6.03	5.98	4.36	4.38	2.08	2.09
P_{loss} (W)	328.44	325.47	283.72	284.15	110.50	110.89
T_{ripple} (%)	83.34	85.94	51.75	52.98	114.90	112.76
T_{avg} error	0.83%		0.46%		0.48%	
P_{loss} error	0.90%		0.15%		0.35%	
T_{ripple} error	3.13%		2.4%		1.86%	

The values of the three optimization objectives between the Kriging model and FEM are shown in Table IV. Detailed errors between the Kriging model and FEM of Point 1, Point 2 and Point 3 are listed in Table IV. The maximum errors of torque, loss, and torque ripple of these three points are only 0.83%, 0.90%, and 3.13%, respectively, and they are acceptable. It can be found that for each point, the error of torque ripple is higher than the other objectives for that the calculation of torque ripple relies on the maximum, average, and minimum values of torque.

E. *Results comparison*

After verification of the Kriging model, it is credible of the optimal solutions selected in Fig. 7. As mentioned above, the results of the selected three optimal solutions are shown in Table III. To clearly show the difference between the initial and the optimal solutions, an optimal solution which exhibits the approximate average torque has been selected from Fig. 7(c). The comparisons of torque and current are displayed in Fig. 8. From Fig. 8(a), it can be seen that the select optimal solution with approximate average output torque exhibits a smaller torque ripple than the initial design. Besides, the current curve of the optimal solution is more reasonable compared with that of the initial design, as shown in Fig. 8(b). Detailed comparison of values between the initial design and the selected optimal solution with approximate output torque is listed in Table V.

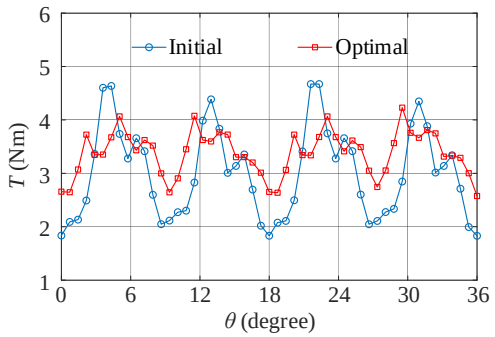

(a)

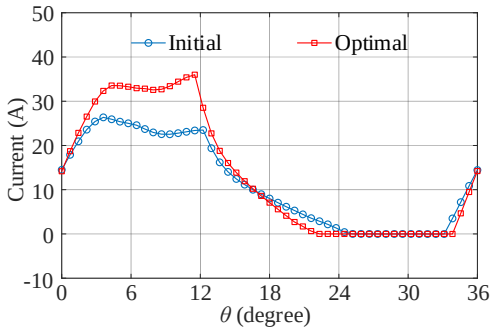

(b)

Fig. 8. Comparison of (a) torque and (b) current between the initial and optimal solutions.

TABLE V
COMPARISON FOR THE APPROXIMATE POWER

Par.	Unit	Initial	Optimal
D_{ro}	mm	82.00	84.79
β_{s1}	deg.	21.38	21.50
β_{s2}	deg.	10.69	9.27
β_r	deg.	26.64	26.62
L_{sy}	mm	7.00	9
h_{cr}	mm	5.5	4.10
g	mm	0.25	0.35
N	-	24	22
θ_{on}	deg.	-3.00	-2.5
θ_{off}	deg	12.00	11.14
T_{avg}	Nm	3.03	3.37
P_{out}	kW	1.90	2.12
P_{loss}	W	195.06	211.67
η	%	90.69	90.92
T_{ripple}	%	93.64	47.84

From these tables, several conclusions can be drawn as follows.

1) Point 1: Compared with the initial design, Point 1 in the region (5~7 Nm) can greatly improve the output power and keep the high efficiency. Besides, the torque ripple can be a little reduced.

2) Point 2: The torque ripple can be greatly reduced step by step by using the proposed method, especially in region 2 (3~5 Nm). The values of torque ripple in this area are lower than 60%. For example, the torque ripple value of Point 2 is only 56.6% of that of the initial design, and the selected optimal solution for comparison with the initial design only has a 47.84% value of torque ripple.

3) Point 3: The torque ripple in region 3 (1~3 Nm) is higher than in the other two regions. However, when the motor is applied to a lower torque condition, it can also keep high efficiency.

4) The multiobjective optimization method provides alternative solutions with a wide range of torque. As shown in Tables III and IV, the toques of Point 1, Point 2, and Point 3 are 6.03 Nm, 4.36 Nm, and 2.08 Nm, respectively. These points can be selected for different applications with demands of different rated torque.

5) For the approximate output power, although the model after optimization exhibits similar efficiency, the torque ripple can be greatly reduced. The torque value of this optimal solution is 47.84%, which is much lower than 93.64% of the initial design. It means the proposed method in which the torque ripple is considered as one of the objectives can greatly reduce the problem of high ripple without the sacrifice of torque and efficiency.

V. Conclusion

In this paper, a comprehensive optimization method consists of multiobjective, system-level, and multilevel methods was presented for SRM drive systems. The proposed method aims to provide a fast way to achieve the best performance of the SRM drive system. An example of an SSRM and its APC control method was investigated to show the effectiveness of the proposed method. Three optimization objectives, i.e., torque, loss, and torque ripple, were selected. To improve the overall performance of the system and reduce the computation cost, all the parameters of the motor and controller have been considered together and divided into three optimization levels by using the sensitivity analysis. The accuracy of the FEM and the Kriging model is verified successively. The proposed method can provide a set of optimal solutions for situations with different output power demands. The solutions obtained from the proposed method exhibit many benefits, including high efficiency and low torque ripple.

References

[1] B. Bilgin, A. Emadi, and M. Krishnamurthy, "Design considerations for switched reluctance machines with a higher number of rotor poles," *IEEE Trans. Ind. Electron.*, vol. 59, no. 10, pp. 3745-3756, 2012.

[2] X. Sun, K. Diao, G. Lei, Y. Guo, and J. Zhu, "Real-time HIL emulation for a segmented-rotor switched reluctance motor using a new magnetic equivalent circuit," *IEEE Trans. Power Electron.*, vol. 35, no. 4, pp. 3841-3849, 2020.

[3] T. Husain, A. Elrayyah, Y. Sozer, and I. Husain, "Unified control for switched reluctance motors for wide speed operation," *IEEE Trans. Ind. Electron.*, vol. 66, no. 5, pp. 3401-3411, 2019.

[4] J. Bayless, N. Kurihara, H. Sugimoto, and A. Chiba, "Acoustic noise reduction of switched reluctance motor with reduced RMS current and enhanced efficiency," *IEEE Trans. Energy Convers.*, vol. 31, no. 2, pp. 627-636, 2016.

[5] K. Diao, X. Sun, G. Lei, G. Bramerdorfer, Y. Guo, and J. Zhu, "System-level robust design optimization of a switched reluctance motor drive system considering multiple driving cycles," *IEEE Trans. Energy Convers.*, DOI: 10.1109/TEC.2020.3009408.

[6] X. Sun, C. Hu, G. Lei, Y. Guo, and J. Zhu, "State feedback control for a PM hub motor based on gray wolf optimization algorithm," *IEEE Trans. Power Electron.*, vol. 35, no. 1, pp. 1136-1146, 2020.

[7] X. Zhu, D. Fan, L. Mo, Y. Chen, and L. Quan, "Multiobjective optimization design of a double-rotor flux-switching permanent magnet machine considering multimode operation," *IEEE Trans. Ind. Electron.*, vol. 66, no. 1, pp. 641-653, 2019.

[8] X. Sun, K. Diao, G. Lei, Y. Guo, and J. Zhu, "Study on segmented-rotor switched reluctance motors with different rotor pole numbers for BSG system of hybrid electric vehicles," *IEEE Trans. Veh. Technol.*, vol. 68, no. 6, pp. 5537-5547, 2019.

[9] D. Wang, X. Du, D. Zhang, and X. Wang, "Design, optimization, and prototyping of segmental-type linear switched-reluctance motor with a toroidally wound mover for vertical propulsion application," *IEEE Trans. Ind. Electron.*, vol. 65, no. 2, pp. 1865-1874, 2018.

[10] X. Sun, K. Diao, and Z. Yang, "Performance improvement of a switched reluctance machine with segmental rotors for hybrid electric vehicles," *Comput. Electr. Eng.*, vol. 77, pp. 244-259, 2019.

[11] E. Silvas, T. Hofman, N. Murgovski, L. F. P. Etman, and M. Steinbuch, "Review of optimization strategies for system-level design in hybrid electric vehicles," *IEEE Trans. Veh. Technol.*, vol. 66, no. 1, pp. 57-70, 2017.

[12] A. S. Mohammadi, J. P. F. Trovão, and C. H. Antunes, "Component-level optimization of hybrid excitation synchronous machines for a specified hybridization ratio using NSGA-II," *IEEE Trans. Energy Convers.*, DOI: 10.1109/TEC.2020.2990283.

[13] C. Ma and L. Qu, "Multiobjective optimization of switched reluctance motors based on design of experiments and particle swarm optimization," *IEEE Trans. Energy Convers.*, vol. 30, no. 3, pp. 1144-1153, 2015.

[14] S. Li, S. Zhang, T. G. Habetler, and R. G. Harley, "Modeling, design optimization, and applications of switched reluctance machines—a review," *IEEE Trans. Ind. Appl.*, vol. 55, no. 3, pp. 2660-2681, 2019.

[15] G. Lei, T. Wang, Y. Guo, J. Zhu, and S. Wang, "System-level design optimization methods for electrical drive systems: deterministic approach," *IEEE Trans. Ind. Electron.*, vol. 61, no. 12, pp. 6591-6602, 2014.

[16] K. Diao, X. Sun, G. Lei, Y. Guo, and J. Zhu, "Multiobjective system level optimization method for switched reluctance motor drive systems using finite element model," *IEEE Trans. Ind. Electron.*, DOI: 10.1109/TIE.2019.2962483.